Draft version February 19, 2026
Typeset using LaTeX twocolumn style in AASTeX631

Supermassive black holes swallow stellar objects at high rates: from Little Red Dots to Black Hole Stars

Konstantinos Kritos [1] and Joseph Silk [1,2,3]

[1] William H. Miller III Department of Physics and Astronomy, Johns Hopkins University, 3400 North Charles Street, Baltimore, Maryland 21218, USA
[2] Institut d'Astrophysique de Paris, UMR 7095 CNRS and UPMC, Sorbonne Université, F-75014 Paris, France
[3] Department of Physics, Beecroft Institute for Particle Astrophysics and Cosmology, University of Oxford, Oxford OX1 3RH, United Kingdom

(Dated: February 19, 2026)

ABSTRACT

Supermassive black hole growth plausibly occurs via runaway astrophysical black hole mergers in nuclear star clusters that form intermediate mass black hole seeds at high redshifts. Such a model of Little Red Dots yields an order-of-magnitude higher rate of tidal disruption events than that of black hole captures. Our prediction, normalised to our proposed resolution of SMBH seeding, yields detectable TDE rates at high redshift. The resulting dense gas cocoons generate the nuclei of LRDs, each incorporating a central massive black-hole-star, with comparable masses in gas, stars, and massive black hole within a scale of around a parsec as inferred from the various spectral signatures.

1. INTRODUCTION

Extreme nuclear transients (ENTs) are rare, ultra-luminous flares ($> 10^{45}\,\mathrm{erg\,s^{-1}}$), exceeding supernova energies and more easily detected at $z > 1$ than classical tidal disruption events (TDEs) in flux-limited surveys. The JWST has also uncovered numerous "Little Red Dots" (LRDs; $4 < z < 8$), likely AGN powered by $\sim 10^7$–$10^8\,M_\odot$ supermassive black holes (SMBHs) (Matthee et al. 2024; Maiolino et al. 2024; Greene et al. 2024).

ENTs show slow decays ($\gtrsim 150\,\mathrm{days}$), emit more total energy than TDEs, and have smooth ($< 10\%$ variability) light curves, blue spectra, and broad lines distinguishing them from AGN variability or supernovae (Frederick et al. 2021). They are proposed to be TDEs of high-mass stars ($> 3\,M_\odot$) by SMBHs (Hinkle et al. 2025).

Typical TDE durations are 3×10^6–10^7 sec (Melchor et al. 2025). Rates are $\sim 10^{-5}\,\mathrm{galaxy^{-1}\,yr^{-1}}$ in normal galaxies, enhanced by 10–100 times in post-starburst systems (van Velzen et al. 2020). A new class of ambiguous nuclear transients (ANTs) is also observed (Wiseman et al. 2025).

Bellovary (2025) estimate a high-z TDE rate of $\sim 10^{-4}\,\mathrm{yr^{-1}}$ (for $5 < z < 8$) by linking LRDs to SMBH-seed densities assuming purely TDE-powered emission, a rate too low for SMBH growth and implying LRD masses below earlier claims. A $\sim 10^7\,M_\odot$ BH has meanwhile been directly measured in a lensed $z = 7$ LRD (Juodžbalis et al. 2025). Since LRDs are likely AGN-dominated, Kritos & Silk (2025) show that including SMBH-growth needs (mergers + accretion) significantly boosts high-z TDE rates, which we argue here may be observable.

In this work, we consider an N-body snapshot of an NSC with a central SMBH and compute the instantaneous TDE and compact-object capture rates in the system, accounting for loss-cone physics and stellar evolution.

2. STELLAR FEEDING ONTO CENTRAL HOLE

We model a nuclear star cluster (NSC) around an SMBH of mass $M_{\rm SMBH}$ and dimensionless spin parameter $a_{\rm SMBH}$. A star of mass $m_\star$ and radius $R_\star$ is removed if its pericenter lies within the loss-cone radius $r_{\rm lc} = \max(r_{\rm T}, r_{\rm mb})$, where $r_{\rm T} = R_\star (M_{\rm SMBH}/m_\star)^{1/3}$ (Evans & Kochanek 1989) and $r_{\rm mb}$ is the spin-dependent marginally bound orbit. For $r_{\rm T} \gtrsim r_{\rm mb}$, the event produces an electromagnetic TDE (Mummery 2023). Stars enter the loss cone via relaxation and are removed on a crossing time.

We compute event rates with Monte Carlo simulations in the Keplerian potential $\Phi = -GM_{\rm SMBH}/r$ within

kkritos1@jhu.edu

the influence radius $r_{\rm infl}$, containing $N_\star \simeq 2M_{\rm SMBH}/\overline{m}_\star$ stars. Stellar masses are drawn from an initial mass function (IMF) and evolved with `updated-BSE` (Banerjee et al. 2020). Assuming $n_\star \propto r^{-\gamma}$ we sample radii from $p(r) \propto r^{3-\gamma}$ and orbits from the isotropic distribution $f(a, e) \propto a^{2-\gamma}e$ (Merritt 2013, Eq. 4.36). Orbital periods follow from Kepler's law, $P \simeq 2\pi GM_{\rm SMBH}m_\star(-E)^{-3/2}$.

Angular-momentum diffusion is driven by non-resonant relaxation (NRR) with a timescale (Merritt 2013, Eq. 5.61)

$$t_{\rm NRR} \simeq \frac{1.8\,{\rm Gyr}}{\ln\Lambda}\frac{10^7\,M_\odot\,{\rm pc}^{-3}}{\rho_\star}\frac{1\,M_\odot}{m}\left(\frac{\sigma_\star}{100\,{\rm km\,s^{-1}}}\right)^3, \quad (1)$$

where $\sigma_\star = (1+\gamma)^{-1/2}(GM_{\rm SMBH}/r)^{1/2}$ and $\ln\Lambda \simeq \ln N_\star$. In the Keplerian regime, we also include resonant relaxation (RR) (Rauch & Tremaine 1996; Gurkan & Hopman 2007), with an effective relaxation time $t_{\rm R} = (t_{\rm NRR}^{-1} + t_{\rm RR}^{-1})^{-1}$ (Hopman & Alexander 2006a, Eq. 11).

Feeding rates are computed using the loss-cone theory by Syer & Ulmer (1999). Defining $\theta_{\rm D} = (P/t_{\rm R})^{1/2}$ (Frank & Rees 1976, Eq. 12), the loss cone is empty for $\theta_{\rm lc} > \theta_{\rm D}$, with rate $[\ln(2/\theta_{\rm lc})t_{\rm R}]^{-1}$, and full otherwise, with rate $\theta_{\rm lc}^2/P$ per unit star. Summing over stars within $r_{\rm infl}$ yields the total instantaneous rate $\Gamma_{\rm lc}(t|M_{\rm SMBH})$.

For compact objects, we additionally include capture by gravitational bremsstrahlung (Quinlan & Shapiro 1989, Eq. 11) and GW-driven inspirals (EMRIs). The effective loss-cone radius is the maximum of tidal, bremsstrahlung, and marginally bound radii. For EMRIs, $\theta_{\rm D} = (t_{\rm GW}/t_{\rm R})^{1/2}$ and the full-loss-cone regime is absent (Alexander & Hopman 2003). We compute $t_{\rm GW}$ using the fit of Mandel (2021).

3. INITIAL CONDITIONS

We adopt a canonical IMF spanning 0.08–150 $M_\odot$ at metallicity $Z = 0.002$. Stellar types from `updated-BSE` are grouped into stellar classes as "MS" (1–2), "giants" (3–6), "cores" (7–9), "WDs" (10–12), "NSs" (13), and "BHs" (14).

Orbits are initialized with a thermal eccentricity distribution; departures from thermal (e.g., superthermal) enhances captures and inspirals by increasing the low-angular-momentum population.

We assume approximate energy equipartition within $r_{\rm infl}$, leading to mass segregation (Hopman & Alexander 2006b). Stars, WDs, and NSs follow density slopes $\gamma_\star = 1.5$, while stellar-mass BHs are more centrally concentrated with $\gamma_{\rm BH} = 2$.

Five representative time epochs (10^0, 10^1, 10^2, 10^3, 10^4 Myr) and three SMBH masses (10^5, 10^6, $10^7\,M_\odot$) are considered with $a_{\rm SMBH} = 0.5$. We link $r_{\rm infl} = GM_{\rm SMBH}/\sigma^2$ to $M_{\rm SMBH}$ through the $M_{\rm SMBH}$–σ relation (McConnell et al. 2011, Fig. 3). We assume the SMBH influence region is fully populated ($M_\star \gtrsim M_{\rm SMBH}$); otherwise, rates would scale down accordingly.

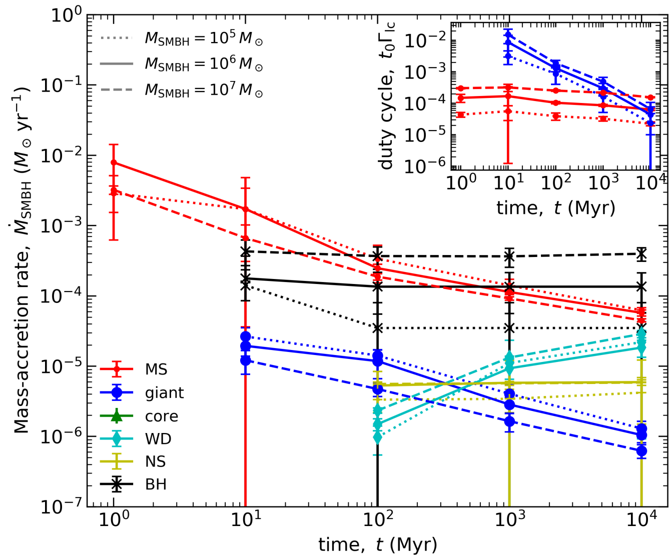

Figure 1. Temporal mass accretion rates from captures onto $10^5\,M_\odot$ (dotted), $10^6\,M_\odot$ (solid), and $10^7\,M_\odot$ (dashed) SMBHs, decomposed by stellar type via loss-cone contributions. Abbreviations: MS (main sequence); WD (white dwarf); NS (neutron star); BH (black hole). Points with error bars indicate mean values and standard deviations from ten realizations. The inset displays the duty cycle of MS (red) and giant (blue) stars.

4. MASS ACCRETION RATE

Figure 1 shows the SMBH mass accretion rate by stellar type. Means and standard deviations are computed from ten realizations per time bin. Assuming a fraction $f_{\rm acc}$ of a stellar mass m is accreted upon loss-cone entry, the accretion rate is $\dot{M}_{\rm SMBH} = f_{\rm acc}\, m\, \Gamma_{\rm lc}^{\rm (A)}(t|M_{\rm SMBH})$ where A is the stellar class. We adopt $f_{\rm acc} = 0.5$ for MS stars (TDEs), $f_{\rm acc} = 0.5$ for giants (envelope disruption), and $f_{\rm acc} = 1$ for compact remnants (BHs, NSs, WDs).

During the first ~ 100 Myr, growth is dominated by MS stars, peaking at $\sim 10^{-2}\,M_\odot\,{\rm yr}^{-1}$ and initially driven by stars $\gtrsim 10\,M_\odot$. At later times ($t \gtrsim 100$ Myr), massive stars evolve into remnants and the disrupted MS population shifts to $\lesssim 10\,M_\odot$. Despite their larger loss cones, giants contribute ~ 2.5 orders of magnitude less mass than MS stars due to short lifetimes and limited envelope masses, becoming negligible at late times.

MS and giant TDEs produce electromagnetic transients. The MS duty cycle (remnant decay time × loss-cone rate) remains $\sim 10^{-4}$, while giants reach $\sim 1\%$ owing to longer decay times, declining below the MS level after several Gyr.

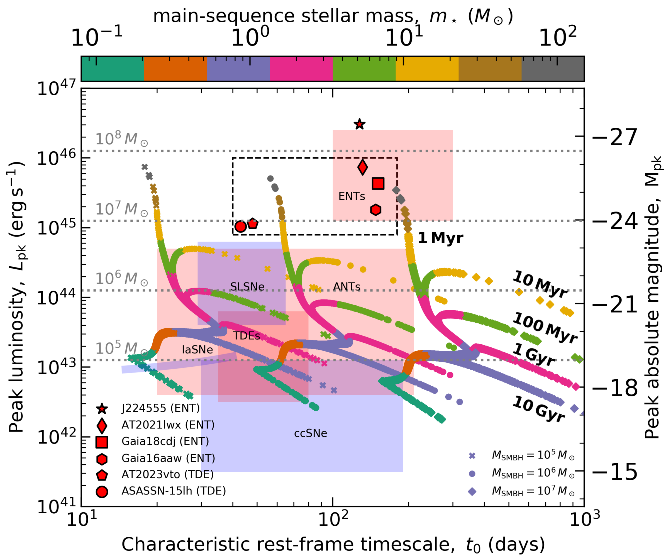

Figure 2. Peak luminosity versus characteristic rest-frame time-scale of astronomical transients, with peak absolute magnitudes normalized to a solar V-band magnitude of 4.83; $\mathrm{M_{pk}} = 2.5 \log_{10}(L_{\rm pk}/L_\odot) - 4.83$. Tidal disruption flares of MS stars by SMBHs of $10^5\,M_\odot$ (crosses), $10^6\,M_\odot$ (circles), and $10^7\,M_\odot$ (diamonds) are shown as colored symbols, with the color bar indicating stellar mass. Five distinct sets correspond to five evolutionary times (bold labels). The six red symbols denote observed flares with $L_{\rm pk} > 10^{45}\,\mathrm{erg\,s^{-1}}$. Gray dotted horizontal lines mark the Eddington luminosities for the labeled SMBH masses. Abbreviations: ENTs (extreme nuclear transients); SLSNe (superluminous supernovae); ANTs (ambiguous nuclear transients); TDEs (tidal disruption events); ccSNe (core-collapse supernovae); IaSNe (Type Ia supernovae) following the Phillips relationship.

A few Myr after stellar-mass BH formation, the total accretion rate stabilizes at $\sim 10^{-4}\,M_\odot\,\mathrm{yr}^{-1}$ for a $10^6\,M_\odot$ SMBH and is higher by a factor of a few for $10^7\,M_\odot$. Accretion is dominated by direct plunges, with negligible inspirals. BHs dominate the late-time growth and contribute significantly even at early times due to mass segregation and their higher masses. WD accretion builds up over several Gyr to just below the MS contribution, while NSs maintain an approximately constant rate of $\sim 5 \times 10^{-6}\,M_\odot\,\mathrm{yr}^{-1}$ after $\sim$ 10–100 Myr. Naked cores are negligible because of their short lifetimes and small radii.

Integrating $\dot{M}_{\rm SMBH}$ over $t \in [0, 1]$ Gyr yields total mass growths of $\simeq 3.9$, 0.45, and 0.057 times the initial SMBH mass for 10^5, 10^6, and $10^7\,M_\odot$, respectively. The cumulative growth scales approximately as $\propto \sqrt{t}$ (also Stone et al. 2017). These values represent upper limits, as relaxation-driven ejections are neglected.

5. FLARING EVENTS

The SMBH disrupts MS stars, while giant-star TDEs are typically partial and involve only envelope stripping (Navarro & Piran 2025). The characteristic flare timescale is the fallback time (Gezari 2021, Eq. 4),

$$t_0 \simeq 40\,\mathrm{days}\,\frac{1\,M_\odot}{m_\star}\left(\frac{R_\star}{R_\odot}\right)^{3/2}\left(\frac{M_{\rm SMBH}}{10^6\,M_\odot}\right)^{1/2}, \quad (2)$$

corresponding to the orbital period of the most bound debris. We adopt the shock-powered emission model of Krolik et al. (2025), in which stream self-intersections near apocenter produce radiation with efficiency (Krolik et al. 2025, Eq. 10)

$$\eta \simeq 4.5 \times 10^{-4}\left(\frac{M_{\rm SMBH}}{10^6\,M_\odot}\right)^{1/3}\left(\frac{m_\star}{1\,M_\odot}\right)^{2/3}\frac{R_\odot}{R_\star}. \quad (3)$$

A complete predictive theory of TDE emission remains uncertain (e.g., Mummery et al. 2025).

Owing to their large radii, giant-star TDEs produce longer, dimmer flares; we therefore restrict our analysis to MS TDEs. Dense cores, naked cores, and WDs can only be disrupted by intermediate-mass BHs (Maguire et al. 2020).

In the efficient-cooling limit ($t_{\rm cool} \ll t_0$), the peak luminosity equals the dissipation rate (Krolik et al. 2025, Eq. 16),

$$L_{\rm pk} \simeq 7.8 \times 10^{43}\,\mathrm{erg\,s^{-1}}\left(\frac{\eta}{4.5 \times 10^{-4}}\right)\frac{m_\star}{1\,M_\odot}\frac{40\,\mathrm{d}}{t_0}, \quad (4)$$

well below $L_{\rm Edd} \simeq 1.2 \times 10^{45}\,\mathrm{erg\,s^{-1}}(M_{\rm SMBH}/10^6\,M_\odot)$. For inefficient cooling ($t_{\rm cool} \gg t_0$), $L_{\rm pk} \sim L_{\rm Edd}$ and the flare duration is $t_0 \simeq m_\star c^2/L_{\rm pk}$ (Krolik et al. 2025, Eq. 18).

Figure 2 shows the peak luminosities and rest-frame decay times of MS TDEs in the efficient-cooling limit, colored by stellar mass, alongside observed transient classes and six extreme flares (Hinkle et al. 2025; Graham et al. 2025). The most luminous events arise from the most massive MS stars. As the stellar population evolves, the maximum MS mass decreases while stellar radii increase near turnoff, producing a late-time turnover since $t_0 \propto R_\star^{3/2}$. TDEs of $\sim$ 30–150 $M_\odot$ MS stars by 10^6–$10^7\,M_\odot$ SMBHs are consistent with ENTs, while lower-mass systems fall in the ANT regime.

6. INTEGRATION OVER COSMOLOGICAL VOLUME

We focus on the redshift range $z < 6$. Assuming a constant SMBH mass function with comoving number density $n_{\rm SMBH}$, we weight three representative SMBH masses by $w_j \propto M_{{\rm SMBH},j}^{-2}$ and normalize $\sum_j w_j = 1$.

The source-frame loss-cone rate density for class A is

$$\mathcal{R}_{\rm lc}^{(\rm A)} \simeq \frac{n_{\rm SMBH}}{10^{-2}\,{\rm Mpc}^{-3}} \sum_{k=1}^{5}\sum_{j=1}^{3} w_j \frac{\Gamma_{\rm lc}^{(\rm A)}(t_k|M_{{\rm SMBH},j})}{10^{-5}\,{\rm yr}^{-1}} \times 20\,{\rm Gpc}^{-3}\,{\rm yr}^{-1}, \tag{5}$$

including both captures and inspirals, and assuming a uniform time prior.

The observer-frame rate follows from integrating over comoving volume and applying cosmological time dilation (Kritos & Silk 2025, Eq. 27). Assuming $\mathcal{R}_{\rm lc}^{(\rm A)}$ is constant over $0 \le z \le 6$,

$$R_{\rm lc}^{(\rm A)} \simeq \frac{\mathcal{R}_{\rm lc}^{(\rm A)}}{20\,{\rm Gpc}^{-3}\,{\rm yr}^{-1}} \frac{\int_{z=0}^{z=6}(1+z)^{-1}dV_{\rm com}(z)}{6.9\times 10^{11}\,{\rm Mpc}^3} \times 1.4\times 10^4\,{\rm yr}^{-1}, \tag{6}$$

scaling linearly with $n_{\rm SMBH}$. Rates are summarized in Table 1.

A	$\mathcal{R}_{\rm capture}$ (${\rm Gpc}^{-3}\,{\rm yr}^{-1}$)	$R_{\rm capture}$ (${\rm yr}^{-1}$)	$\mathcal{R}_{\rm inspiral}$ (${\rm Gpc}^{-3}\,{\rm yr}^{-1}$)	$R_{\rm inspiral}$ (${\rm yr}^{-1}$)
MS	5.4×10^3	3.8×10^6	4.7×10^{-6}	4.4×10^{-2}
giant	1.5×10^2	1.1×10^5	1.6×10^{-7}	3.3×10^{-3}
WD	8.6×10^1	6.0×10^4	4.9×10^{-8}	1.5×10^{-3}
NS	1.5×10^1	1.0×10^4	1.1×10^{-10}	9.9×10^{-7}
BH	2.2×10^1	1.5×10^4	2.8×10^{-7}	1.9×10^{-2}

Table 1. Capture and inspiral loss-cone density and volume-integrated rates over $0 \le z \le 6$ for different stellar classes.

The total SMBH mass growth over $z \in [0, 6]$ is

$$\approx \frac{n_{\rm SMBH}}{10^{-2}\,{\rm Mpc}^{-3}} \sum_{j=1}^{3} w_j \frac{\int_0^{10\,{\rm Gyr}} dt\,\dot{M}_{{\rm SMBH},j}(t)}{1.8\times10^6\,M_\odot} \times 1.8\cdot 10^{13}\,M_\odot\,{\rm Gpc}^{-3} \tag{7}$$

which is on the same order of Sołtan's estimated mass density ($8\times10^{13}\,M_\odot\,{\rm Gpc}^{-3}$, Soltan 1982), implying gas accretion dominates SMBH growth but loss-cone effects contribute at the $\sim 25\%$ level.

We find an MS TDE rate of $\approx 5\times10^3\,{\rm Gpc}^{-3}\,{\rm yr}^{-1}$ at $4 \le z \le 6$, with only a small detectable fraction (e.g. UVEX; Kulkarni et al. 2021) while inspirals are negligible in all classes. For comparison, the local TDE rate density is $\sim$ 15–200 ${\rm Gpc}^{-3}\,{\rm yr}^{-1}$ (van Velzen & Farrar 2014), below theoretical $z \sim 0$ expectations (Stone & Metzger 2016), while recent candidates at $z > 1$ (Gu et al. 2025) imply rates of $\sim$ 20–80 ${\rm Gpc}^{-3}\,{\rm yr}^{-1}$ at $z \sim 1$ (Graham et al. 2025). In addition, $\mathcal{R}_{\rm MS} : \mathcal{R}_{\rm giant} \sim 30$. Finally, stellar remnants capture at intrinsic rates of hundreds per year, and about two BH-EMRI every century, producing GW sources, which we discuss next.

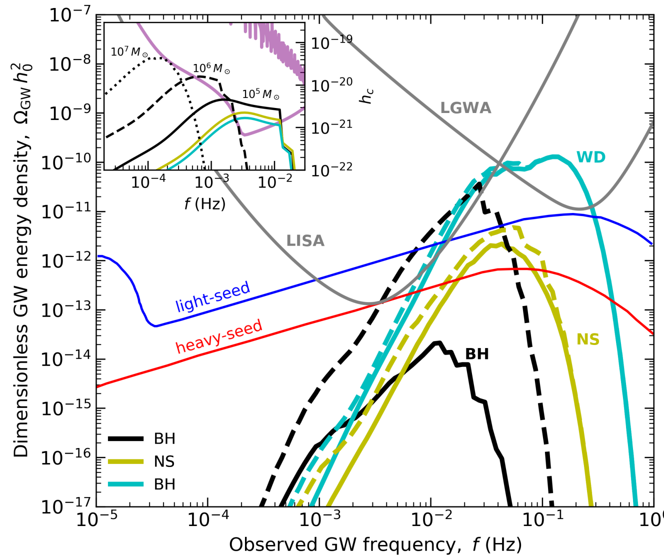

Figure 3. Total dimensionless gravitational-wave (GW) energy density from BH (black), NS (yellow), and WD (cyan) captures within $z < 6$ as a function of the observed GW frequency. The comoving SMBH number density is assumed constant at $10^{-2}\,{\rm Mpc}^{-3}$. Gray curves indicate the PLS of LISA and LGWA with an SNR = 10 and $T_{\rm obs} = 4\,{\rm yr}$. Also shown are the GW backgrounds from mergers of massive BHs under the light- and heavy-seed scenarios (Çalışkan et al. 2025). The inset shows the characteristic strain for a few $z \sim 5$ captures.

7. GRAVITATIONAL-WAVE BACKGROUND

We compute the characteristic GW strain of each capture, $h_c(f)$, at the observer-frame frequency f, using Eq. (17) of Bonetti & Sesana (2020), including the first 100 harmonics. Merger–ringdown and spin effects are neglected. Example individual sources at $z \sim 5$ are shown in the inset of Fig. 3 together with the sensitivities of LGWA (Harms et al. 2021) and LISA (Amaro-Seoane et al. 2017). Captures originate from highly eccentric ($e \simeq 1^-$) orbits that rapidly circularize and merge within $\simeq 28\,{\rm min}\,M_{\rm SMBH}/(10^6\,M_\odot)(10\,{\rm km\,s^{-1}}/\sigma)^3$ (O'Leary et al. 2009). We find that $\simeq 54\%$ ($\simeq 1.3\%$), $\simeq 7.9\%$ ($\simeq 0.6\%$), and $\simeq 3.3\%$ ($\simeq 0.5\%$) of all BH, NS, and WD captures, respectively, have SNR > 10 in LISA (LGWA).

The cumulative contribution of captures produces a stochastic GW background (SGWB), whose dimensional energy density over an observation time $T_{\rm obs}$ we approximate as (Belgacem et al. 2025, Eq. 3.83)

$$\Omega_{\rm lc}^{(\rm A)}(f)h_0^2 = \frac{1\,{\rm yr}}{{\rm T_{obs}}}\left(\frac{f}{10^{-2}\,{\rm Hz}}\right)^3 \sum_{i=1}^{\tilde{\mathcal{N}}_{\rm A}}\sum_{j=1}^{3} w_j \left[\frac{h_{c,ij}(f)}{10^{-20}}\right]^2 \times 2\cdot 10^{-13}\,\frac{\tilde{\mathcal{N}}_{\rm A}}{10^4}, \tag{8}$$

A = {WD, NS, BH} and h_0 is the reduced Hubble's constant. The sum is over undetectable $\tilde{\mathcal{N}}_{\rm A}$ captures with SNR < 10, by convention.

The resulting SGWBs are shown in Fig. 3 (thick lines). The WD capture background peaks at deciHz and are observable with an SNR > 10 when compared with the corresponding LGWA PLS (Ajith et al. 2025) and LISA PLS (Schmitz 2020) for $T_{\rm obs} = 4\,{\rm yr}$. For comparison, we also show the background from massive black-hole mergers under two seeding scenarios (Çalışkan et al. 2025). While the BH and NS backgrounds have SNR < 10 within four years, there are still thousands of captures within $z < 6$ with LISA. Finally, the SGWB from inspirals is undetectable.

8. FORMATION OF THE BLACK-HOLE STAR

We adopt a BH–star framework in which the SMBH is embedded in a dense cocoon of gas and stars. This model provides a consistent interpretation of LRDs, satisfies spectral constraints, and enables rapid SMBH growth via bursty, super-Eddington gas accretion (Kritos & Silk 2025; Kokorev et al. 2025). The buildup of dense gas cocoons produces extreme Balmer breaks, Balmer absorption, and $H\beta$ emission, identifying LRDs as BH-stars (de Graaff et al. 2025; Naidu et al. 2025); see also (Begelman & Dexter 2026; Nandal & Loeb 2025; Rusakov et al. 2025).

Feedback-regulated growth yields universal scalings: momentum conservation gives $M_{\rm BH} \propto \sigma^4$,

$$f_{\rm Edd}\left(\frac{4\pi G M_{\rm SMBH} c}{\kappa_{\rm es}}\right) = \frac{\epsilon \sigma^4 v_s}{G}, \tag{9}$$

while energy conservation implies $M_{\rm SMBH} \propto \sigma^5$. The SMBH radius of influence, $r_{\rm infl} \sim 10$–$30\,{\rm pc}$, defines the Bondi radius.

Accretion-disk sizes inferred from reverberation mapping are typically parsec-scale. The Eddington feedback region is set by requiring a unit Thomson optical depth,

$$(n_e \sigma_T)^{-1} = m_p M_g^2 G^3 \sigma^{-6} \sigma_T^{-1} \simeq (M_g/M_\odot)^2\, \sigma_{200}^{-6}, \tag{10}$$

using $\rho_g = \sigma^6 G^{-3} M_g^{-2}$ and stellar mass form factors (Diener et al. 1995). This defines a dense central core at radii ~ 1–$10\,{\rm AU}$, consistent with CLOUDY models of inverted LRD spectra and inferred gas densities $n_H \sim 10^8\,{\rm cm}^{-3}$ (Taylor et al. 2025).

Observations and theory favor Comptonization-regulated feedback (Gilli et al. 2022): momentum-driven regulation dominates at high redshift, while energy-driven feedback with momentum boosting becomes important at low redshift, enhancing early star formation and later driving massive outflows (Silk et al. 2024; Costa et al. 2014). Specifically,

- *Momentum-driven feedback:* $M_{\rm BH} \propto \sigma^4(\sigma_T/m_p)/(\pi G^2)$; inverse-Compton cooling yields insufficient momentum by a factor ~ 10, but can trigger positive star-formation feedback (Silk & Nusser 2010).

- *Energy-driven feedback:* $M_{\rm SMBH} = \alpha\sigma^5(\sigma_T/m_p)/(\pi\eta c G^2)$, providing the required momentum boosting and reproducing the observed $M_{\rm BH}$–σ relation.

9. CONCLUSIONS

We modeled stellar feeding onto SMBHs in NSCs, including TDEs and compact-object captures. Stellar plunges contribute only a sizable fraction to SMBH mass growth; however, gas accretion still dominates at all redshifts.

Main-sequence TDEs dominate the electromagnetic output. Disruptions of massive ($\sim$ 30–150 $M_\odot$) stars by 10^6–$10^7\,M_\odot$ SMBHs naturally reproduce the luminosities and timescales of ENTs, while giant-star TDEs are negligible. We predict an intrinsic MS TDE rate of $\sim 5\times10^3\,{\rm Gpc}^{-3}\,{\rm yr}^{-1}$ at $4 \le z \le 6$, though only a small fraction are observable.

Compact-object captures produce thousands of detectable LISA sources within $z < 6$ and generate a stochastic GW background, dominated by WD captures at deciHz frequencies.

Stellar feeding is therefore an inevitable byproduct of dense, rapidly growing high-redshift nuclei; insufficient for SMBH growth, but observable through extreme TDEs and GWs, providing a direct probe of black-hole–star systems and early SMBH assembly.

Our data and code are publicly available at https://zenodo.org/records/18471816.

We thank Mesut Çalışkan, Marco Chiaberge, Muryel Guolo, Francesco Iacovelli, Mithell Karmen, Julian Krolik, and Colin Norman for discussions. K.K. is supported by NSF Grants No. AST-2307146, PHY-2513337, PHY-090003, and PHY-20043, by NASA Grant No. 21-ATP21-0010, by John Templeton Foundation Grant No. 62840, by the Simons Foundation [MPS-SIP-00001698, E.B.], by the Simons Foundation International, by Italian Ministry of Foreign Affairs and International Cooperation Grant No. PGR01167, and Onassis Foundation Scholarship (ID: F ZT 041-1/2023-2024).

t (Myr)	1	10	100	1,000	10,000
MS	$(6.7 \pm 1.2) \times 10^{-4}$	$(7 \pm 2) \times 10^{-4}$	$(5.3 \pm 1.0) \times 10^{-4}$	$(4.3 \pm 0.5) \times 10^{-4}$	$(3.4 \pm 0.6) \times 10^{-4}$
giant	0	$(2.0 \pm 1.3) \times 10^{-5}$	$(1.8 \pm 0.3) \times 10^{-5}$	$(3.1 \pm 1.2) \times 10^{-5}$	$(6.7 \pm 1.3) \times 10^{-6}$
WD	0	0	$(8 \pm 4) \times 10^{-7}$	$(1.3 \pm 1.3) \times 10^{-5}$	$(3 \pm 2) \times 10^{-5}$
NS	0	0	$(2.2 \pm 0.7) \times 10^{-6}$	$(2.3 \pm 0.8) \times 10^{-6}$	$(3 \pm 2) \times 10^{-6}$
BH	0	$(5.2 \pm 0.7) \times 10^{-6}$	$(1.9 \pm 1.8) \times 10^{-6}$	$(1.9 \pm 1.8) \times 10^{-6}$	$(1.9 \pm 1.8) \times 10^{-6}$

Table 2. Capture loss-cone rates onto $M_{\rm SMBH} = 10^5\,M_\odot$ in yr^{-1} at evolution time t for different stellar types. Rates of naked cores are zero. Error bars are standard deviations estimated over ten realizations. Total number of stellar objects within the influence radius is $N_\star = 301,550$. Abbreviations: MS (main sequence); WD (white dwarf); NS (neutron star); BH (black hole).

t (Myr)	1	10	100	1,000	10,000
MS	$(8 \pm 3) \times 10^{-4}$	$(6 \pm 4) \times 10^{-4}$	$(3.8 \pm 0.2) \times 10^{-4}$	$(3.8 \pm 0.2) \times 10^{-4}$	$(2.4 \pm 0.2) \times 10^{-4}$
giant	0	$(0.5 \pm 0.5) \times 10^{-5}$	$(1.4 \pm 0.2) \times 10^{-5}$	$(2.0 \pm 1.3) \times 10^{-5}$	$(5.3 \pm 1.0) \times 10^{-6}$
WD	0	0	$(1.2 \pm 0.2) \times 10^{-6}$	$(1.0 \pm 0.3) \times 10^{-5}$	$(2.6 \pm 0.6) \times 10^{-5}$
NS	0	0	$(4 \pm 2) \times 10^{-6}$	$(3 \pm 2) \times 10^{-6}$	$(3 \pm 2) \times 10^{-6}$
BH	0	$(9 \pm 4) \times 10^{-6}$	$(1.1 \pm 0.7) \times 10^{-5}$	$(1.1 \pm 0.7) \times 10^{-5}$	$(1.1 \pm 0.7) \times 10^{-5}$

Table 3. Same as Table 2 with $M_{\rm SMBH} = 10^6\,M_\odot$. Total number of stellar objects within the influence radius is $N_\star = 3,015,502$.

t (Myr)	1	10	100	1,000	10,000
MS	$(4.9 \pm 0.2) \times 10^{-4}$	$(4.3 \pm 0.4) \times 10^{-4}$	$(3.5 \pm 0.2) \times 10^{-4}$	$(3.0 \pm 0.1) \times 10^{-4}$	$(2.29 \pm 0.06) \times 10^{-4}$
giant	0	$(1.0 \pm 0.4) \times 10^{-5}$	$(7.4 \pm 1.6) \times 10^{-6}$	$(1.2 \pm 0.1) \times 10^{-5}$	$(3.2 \pm 0.6) \times 10^{-6}$
WD	0	0	$(1.9 \pm 0.2) \times 10^{-6}$	$(1.49 \pm 0.07) \times 10^{-5}$	$(4.2 \pm 0.3) \times 10^{-5}$
NS	0	0	$(3.8 \pm 0.2) \times 10^{-6}$	$(3.8 \pm 0.2) \times 10^{-6}$	$(3.9 \pm 0.4) \times 10^{-6}$
BH	0	$(1.7 \pm 0.6) \times 10^{-5}$	$(1.9 \pm 0.7) \times 10^{-5}$	$(1.8 \pm 0.5) \times 10^{-5}$	$(2.0 \pm 0.3) \times 10^{-5}$

Table 4. Same as Table 2 with $M_{\rm SMBH} = 10^7\,M_\odot$. Total number of stellar objects within the influence radius is $N_\star = 30,155,026$.

APPENDIX

A. EXTENDED TABLES OF LOSS-CONE RATES

This Appendix presents capture loss-cone rates and associated uncertainty for each stellar type at the five different epochs onto a $10^5\,M_\odot$ (Table 2), $10^6\,M_\odot$ (Table 3), and $10^7\,M_\odot$ (Table 4) SMBH.

REFERENCES

Ajith, P., et al. 2025, JCAP, 01, 108, doi: 10.1088/1475-7516/2025/01/108

Alexander, T., & Hopman, C. 2003, ApJL, 590, L29, doi: 10.1086/376672

Amaro-Seoane, P., et al. 2017. https://arxiv.org/abs/1702.00786

Banerjee, S., Belczynski, K., Fryer, C. L., et al. 2020, Astron. Astrophys., 639, A41, doi: 10.1051/0004-6361/201935332

Begelman, M. C., & Dexter, J. 2026, Astrophys. J., 996, 48, doi: 10.3847/1538-4357/ae274a

Belgacem, E., Iacovelli, F., Maggiore, M., Mancarella, M., & Muttoni, N. 2025, JCAP, 04, 032, doi: 10.1088/1475-7516/2025/04/032

Bellovary, J. 2025, Astrophys. J. Lett., 984, L55, doi: 10.3847/2041-8213/adce6c

Bonetti, M., & Sesana, A. 2020, Phys. Rev. D, 102, 103023, doi: 10.1103/PhysRevD.102.103023

Çalışkan, M., Anil Kumar, N., Kamionkowski, M., & Cheng, S. 2025. https://arxiv.org/abs/2506.18965

Costa, T., Sijacki, D., & Haehnelt, M. G. 2014, Mon. Not. Roy. Astron. Soc., 444, 2355, doi: 10.1093/mnras/stu1632

de Graaff, A., Rix, H.-W., Naidu, R. P., et al. 2025, A&A, 701, A168, doi: 10.1051/0004-6361/202554681
Diener, P., Kosovichev, A. G., Kotok, E. V., Novikov, I. D., & Pethick, C. J. 1995, MNRAS, 275, 498, doi: 10.1093/mnras/275.2.498
Evans, C. R., & Kochanek, C. S. 1989, ApJL, 346, L13, doi: 10.1086/185567
Frank, J., & Rees, M. J. 1976, MNRAS, 176, 633, doi: 10.1093/mnras/176.3.633
Frederick, S., et al. 2021, Astrophys. J., 920, 56, doi: 10.3847/1538-4357/ac110f
Gezari, S. 2021, Ann. Rev. Astron. Astrophys., 59, 21, doi: 10.1146/annurev-astro-111720-030029
Gilli, R., Norman, C., Calura, F., et al. 2022, A&A, 666, A17, doi: 10.1051/0004-6361/202243708
Graham, M. J., et al. 2025, doi: 10.1038/s41550-025-02699-0
Greene, J. E., et al. 2024, Astrophys. J., 964, 39, doi: 10.3847/1538-4357/ad1e5f
Gu, Y., Zhang, X.-G., Chen, X.-Q., Yang, X., & Liang, E.-W. 2025, Mon. Not. Roy. Astron. Soc., 537, 84, doi: 10.1093/mnras/stae2816
Gurkan, M. A., & Hopman, C. 2007, Mon. Not. Roy. Astron. Soc., 379, 1083, doi: 10.1111/j.1365-2966.2007.11982.x
Harms, J., et al. 2021, Astrophys. J., 910, 1, doi: 10.3847/1538-4357/abe5a7
Hinkle, J. T., Shappee, B. J., Auchettl, K., et al. 2025, Science Advances, 11, eadt0074, doi: 10.1126/sciadv.adt0074
Hopman, C., & Alexander, T. 2006a, Astrophys. J., 645, 1152, doi: 10.1086/504400
—. 2006b, Astrophys. J. Lett., 645, L133, doi: 10.1086/506273
Juodžbalis, I., Marconcini, C., D'Eugenio, F., et al. 2025, arXiv e-prints, arXiv:2508.21748, doi: 10.48550/arXiv.2508.21748
Kokorev, V., Chisholm, J., Naidu, R. P., et al. 2025, arXiv e-prints, arXiv:2511.07515, doi: 10.48550/arXiv.2511.07515
Kritos, K., & Silk, J. 2025. https://arxiv.org/abs/2510.21709
Krolik, J., Piran, T., & Ryu, T. 2025, Astrophys. J., 988, 220, doi: 10.3847/1538-4357/ade797
Kulkarni, S. R., et al. 2021. https://arxiv.org/abs/2111.15608
Maguire, K., Eracleous, M., Jonker, P. G., MacLeod, M., & Rosswog, S. 2020, Space Sci. Rev., 216, 39, doi: 10.1007/s11214-020-00661-2
Maiolino, R., et al. 2024, Astron. Astrophys., 691, A145, doi: 10.1051/0004-6361/202347640
Mandel, I. 2021, Res. Notes AAS, 5, 223, doi: 10.3847/2515-5172/ac2d35
Matthee, J., et al. 2024, Astrophys. J., 963, 129, doi: 10.3847/1538-4357/ad2345
McConnell, N. J., Ma, C.-P., Gebhardt, K., et al. 2011, Nature, 480, 215, doi: 10.1038/nature10636
Melchor, D., Naoz, S., Gezari, S., & Mockler, B. 2025, Astrophys. J. Lett., 992, L21, doi: 10.3847/2041-8213/ae0a2e
Merritt, D. 2013, Dynamics and evolution of galactic nuclei (Princeton, NJ: Princeton University Press)
Mummery, A. 2023, Mon. Not. Roy. Astron. Soc., 527, 6233, doi: 10.1093/mnras/stad3636
Mummery, A., Metzger, B., van Velzen, S., & Guolo, M. 2025. https://arxiv.org/abs/2512.09143
Naidu, R. P., et al. 2025. https://arxiv.org/abs/2503.16596
Nandal, D., & Loeb, A. 2025, arXiv e-prints, arXiv:2507.12618, doi: 10.48550/arXiv.2507.12618
Navarro, N. N., & Piran, T. 2025, Astrophys. J., 983, 177, doi: 10.3847/1538-4357/ad96b7
O'Leary, R. M., Kocsis, B., & Loeb, A. 2009, Mon. Not. Roy. Astron. Soc., 395, 2127, doi: 10.1111/j.1365-2966.2009.14653.x
Quinlan, G. D., & Shapiro, S. L. 1989, ApJ, 343, 725, doi: 10.1086/167745
Rauch, K. P., & Tremaine, S. 1996, NewA, 1, 149, doi: 10.1016/S1384-1076(96)00012-7
Rusakov, V., Watson, D., Nikopoulos, G. P., et al. 2025, arXiv e-prints, arXiv:2503.16595, doi: 10.48550/arXiv.2503.16595
Schmitz, K. 2020, Symmetry, 12, 1477, doi: 10.3390/sym12091477
Silk, J., Begelman, M. C., Norman, C., Nusser, A., & Wyse, R. F. G. 2024, Astrophys. J. Lett., 961, L39, doi: 10.3847/2041-8213/ad1bf0
Silk, J., & Nusser, A. 2010, Astrophys. J., 725, 556, doi: 10.1088/0004-637X/725/1/556
Soltan, A. 1982, MNRAS, 200, 115, doi: 10.1093/mnras/200.1.115
Stone, N. C., Küpper, A. H. W., & Ostriker, J. P. 2017, Mon. Not. Roy. Astron. Soc., 467, 4180, doi: 10.1093/mnras/stx097
Stone, N. C., & Metzger, B. D. 2016, Mon. Not. Roy. Astron. Soc., 455, 859, doi: 10.1093/mnras/stv2281
Syer, D., & Ulmer, A. 1999, MNRAS, 306, 35, doi: 10.1046/j.1365-8711.1999.02445.x
Taylor, A. J., Kokorev, V., Kocevski, D. D., et al. 2025, ApJL, 989, L7, doi: 10.3847/2041-8213/ade789
van Velzen, S., & Farrar, G. R. 2014, Astrophys. J., 792, 53, doi: 10.1088/0004-637X/792/1/53

van Velzen, S., Holoien, T. W. S., Onori, F., Hung, T., & Arcavi, I. 2020, Space Sci. Rev., 216, 124, doi: 10.1007/s11214-020-00753-z

Wiseman, P., et al. 2025, Mon. Not. Roy. Astron. Soc., 537, 2024, doi: 10.1093/mnras/staf116